Andrzej FIRLIT
AKADEMIA GÓRNICZO–HUTNICZA, WYDZIAŁ ELEKTROTECHNIKI, AUTOMATYKI, INFORMATYKI I ELEKTRONIKI,
KATEDRA AUTOMATYKI NAPĘDU I URZĄDZEŃ PRZEMYSŁOWYCH

Current's physical components theory and *p-q* power theory in the control of the three-phase shunt active power filter

Ph.D. Andrzej FIRLIT

Was born in Tarnów, Poland, in 1971. He received M.Sc. and Ph.D. degrees in electrical engineering from the AGH University of Science and Technology in Kraków, Poland, in 1996 and 2006, respectively. At present he is researcher in this University, in the Institute of Electrical Drive and Industrial Equipment Control. His areas of interest include power quality, power theories, active power filtering and computer analysis of power electronics systems.

e-mail: firlit@kaniup.agh.edu.pl

Abstract

This paper presents the comparison of the control algorithms for a three phase, three wire shunt active power filter. The control algorithms are based on: the current's physical components theory and the *p-q* power theory. The active power filter operation under the distorted supply voltage at the point of common coupling condition is considered. The comparison concerns the aspects of: filtering current harmonics, reactive power compensation (defined in the fundamental harmonic domain), supply current balancing and dynamic performance. The results of the laboratory investigation, using the fast prototyping system dSPACE, are given in the paper.

Keywords: active power filter, power theories, electric power quality.

Teoria składowych fizycznych prądu oraz teoria mocy *p-q* w zastosowaniu do sterowania równoległym energetycznym filtrem aktywnym

Streszczenie

W artykule przedstawiono porównanie algorytmów sterowania trójfazowym, trójprzewodowym równoległym energetycznym filtrem aktywnym. Algorytmy sterowania opracowano na podstawie dwóch teorii mocy: teorii składowych fizycznych prądu oraz teorii mocy *p-q*. Badaniom podlegała praca energetycznego filtru aktywnego w warunkach odkształconego napięcia zasilającego w punkcie wspólnego przyłączenia. Za kryterium porównania przyjęto: filtrację wyższych harmonicznych prądu odbiornika, kompensację mocy biernej (zdefiniowanej w dziedzinie podstawowej harmonicznej), symetryzację asymetrycznych prądów linii zasilającej odbiornik oraz dynamikę energetycznego filtru aktywnego. W artykule zamieszczono wyniki pomiarów i badań otrzymane na zbudowanym stanowisku laboratoryjnym trójfazowego, trójprzewodowego równoległego energetycznego filtru aktywnego z wykorzystaniem systemu szybkiego prototypowania dSPACE.

Słowa kluczowe: energetyczny filtr aktywny, teorie mocy, jakość energii elektrycznej.

1. Introduction

The active power filters (APFs) have been known as one of the best tools for harmonic mitigation as well as reactive power compensation, supply current balancing, voltage regulation and voltage flicker compensation etc. This wide range of objectives is achieved either individually or in combination, depending upon the requirements, a control algorithm (CA) and a configuration which have to be selected appropriately. One of the most popular APFs is shunt APF (SAPF), which is controlled to generate the required compensating currents. The control algorithm (CA) is one of the subsystems of the APF control system. The task of control algorithm is evaluation of reference signals on the grounds of information about voltages and currents at the point of common coupling (PCC). To obtain elimination of undesirable current components the applied control algorithm of SAPF has to evaluate properly the current components corresponding to higher harmonics, reactive power (defined in the fundamental harmonic domain) and the negative sequence components of the load current. The presence of distorted voltage at the PCC could affect evaluation of correct current components values. It depends on the chosen control algorithm. There are a number of methods that enable implementation of the control algorithm of shunt APF (SAPF), in a time or frequency domain. They are based on one of the power theories or the other approaches. This paper presents the comparison of the two control algorithms of SAPF under conditions of distorted voltage. They were designed on the basis of: the *p-q* power theory (PQT) and the current's physical components theory (CPCT). The first one was proposed by H. Akagi, A. Nabae and Y. Kanazawa [1-4], the second one was proposed by L. S. Czarnecki [9-12]. The PQT was developed in time domain, whereas the CPCT was developed in the frequency domain. The PQT is a well-known modern power theory and it is widely used in the field of active filtering, whereas the CPCT hasn't been used in this area yet.

2. Description of the investigated system

The block diagram of the investigated three-phase three-wire SAPF system is shown in Fig. 1. A thyristor rectifier, with *RL* load was used as a non-linear load. The resistor R_{uRS} was connected between the phases *R* and *S* in order to cause load currents unbalance. SAPF configuration is based on a force-commutated pulse-width modulated voltage-source inverter (PWM-VSI) connected to a dc capacitor C_{APF}. The elimination of undesired load current components is achieved by injecting equal but of opposite sign compensating currents $\boldsymbol{i}_{APF}$, which are generated by SAPF according to the chosen control algorithms. SAPF operation with the source non-zero internal impedance Z_S and for distorted voltage at the point of common coupling, resulting from the influence of other loads connected at the PCC, has been considered.

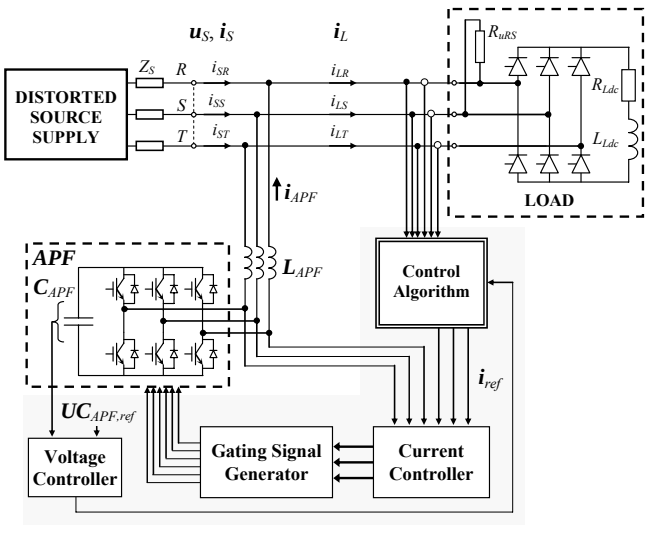

Fig. 1. The structure of the investigated shunt active power filter (SAPF)
Rys. 1. Struktura badanego układu równoległego energetycznego filtru aktywnego (SAPF)

The current controller ensures constant switching frequency f_{sw}. It is essential considering the structure and effectiveness of the switching frequency filter, which eliminates the switching frequency component of SAPF current. For this purpose has been applied the current controller, whose structure is presented in Fig. 2 [18, 25].

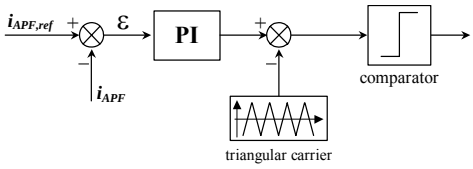

Fig. 2. The block diagram of the current controller
Rys. 2. Schemat blokowy regulatora prądu

A constant switching frequency is achieved by comparing the current error signal ε with a triangular reference waveform. The purpose of introducing the triangular waveform is to stabilize the converter switching frequency by forcing it to be constant and equal to the frequency of the triangular reference signal. The error signal is processed through a PI controller before the comparison with the triangular carrier takes place. Switching of power SAPF produces the current ripples and also voltage ripples at the supply side because of non-zero internal source impedance Z_S. Voltage control of the dc bus is performed by adjusting the small amount of active power flowing into the dc capacitor C_{APF}, thus compensating for both the converter and system losses [25].

3. Control Algorithms

According to the PQT, the current of the three-phase, unbalanced, non-linear load has been expressed into four components[1]

$$\boldsymbol{i} = \boldsymbol{i}_{\overline{p}\mathrm{PQ}} + \boldsymbol{i}_{\overline{q}\mathrm{PQ}} + \boldsymbol{i}_{h\mathrm{PQ}} + \boldsymbol{i}_{2f_{(1)}\mathrm{PQ}} \tag{1}$$

where: $p = \overline{p} + \widetilde{p}_h + \widetilde{p}_{2f_{(1)}}$ – instantaneous real power, $q = \overline{q} + \widetilde{q}_h + \widetilde{q}_{2f_{(1)}}$ – instantaneous imaginary power[2] and $\boldsymbol{i}_{\overline{p}}$ – is associated with $\overline{p}$, i.e. with the active power P defined in the traditional way; $\boldsymbol{i}_{\overline{q}}$ – is associated with $\overline{q}$, i.e. with the reactive power Q (In the case of a balanced sinusoidal supply voltage and balanced load with or without harmonics, $\overline{q}$ is equal to the reactive power Q defined in the traditional way in the fundamental harmonic domain.); $\boldsymbol{i}_h$ – is associated with $\widetilde{p}_h$ and $\widetilde{q}_h$, i.e. with the presence of harmonics in voltage and current waveforms; $\boldsymbol{i}_{2f_{(1)}}$ – is associated with $\widetilde{p}_{2f_{(1)}}$ and $\widetilde{q}_{2f_{(1)}}$, i.e. the unbalance load currents. The block diagram of the tested CA-PQT is shown in Fig. 3a.

According to the CPCT, the current of the three-phase, unbalanced, non-linear load has been decomposed into five components

$$\boldsymbol{i} = \boldsymbol{i}_a + \boldsymbol{i}_s + \boldsymbol{i}_r + \boldsymbol{i}_u + \boldsymbol{i}_B \tag{2}$$

where: $\boldsymbol{i}_a$ – active current, $\boldsymbol{i}_s$ – scattered current, $\boldsymbol{i}_r$ – reactive current, $\boldsymbol{i}_u$ – unbalanced current and $\boldsymbol{i}_B$ – load generated current.

[1] Phase currents and voltages are expressed in the form of column vectors $\boldsymbol{i} = \boldsymbol{i}(t)$ and $\boldsymbol{u} = \boldsymbol{u}(t)$, where $\boldsymbol{i} = [i_R, i_S, i_T]^T$, $\boldsymbol{u} = [u_R, u_S, u_T]^T$

[2] $\overline{p}, \overline{q}$ – average components, $\widetilde{p}_h, \widetilde{q}_h$ – oscillating components (h – „harmonic") and $\widetilde{p}_{2f_{(1)}}, \widetilde{q}_{2f_{(1)}}$ – oscillating components ($2f_{(1)}$ – with double frequency of the fundamental component frequency)

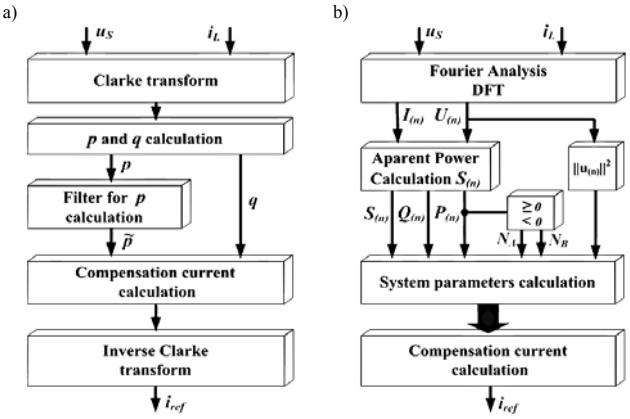

Fig. 3. The block diagrams of the control algorithms: a) CA-PQT and b) CA-CPCT
Rys. 3. Schematy blokowe algorytmów sterowania: a) CA-PQT i b) CA-CPCT

Each component is associated with a different power phenomenon and is orthogonal with respect to the others. Thus the current decomposition (2) reveals five different physical phenomena, which determine the load current value, namely: active power transmission to the load – $\boldsymbol{i}_a$; change of the load conductance $G_{e(\mathrm{n})}$ with frequency – $\boldsymbol{i}_s$; reciprocating flow of energy – $\boldsymbol{i}_r$; load currents unbalance – $\boldsymbol{i}_u$; active power transmission back to the source – $\boldsymbol{i}_B$. If harmonic currents are generated by the supply source, due to the distorted voltage, then the current components $\boldsymbol{i}_a$, $\boldsymbol{i}_s$, $\boldsymbol{i}_r$, $\boldsymbol{i}_u$ may contain, besides the fundamental, also high-order harmonics of the orders already present in the voltage[3]. Thus, each of the components $\boldsymbol{i}_a$, $\boldsymbol{i}_s$, $\boldsymbol{i}_r$, $\boldsymbol{i}_u$ can be additionally decomposed into the fundamental and high-order harmonics, e.g.:

$$\boldsymbol{i}_a = \boldsymbol{i}_{a(1)} + \boldsymbol{i}_{a(\mathrm{h})}, \tag{3}$$

where: the subscript (h) means the harmonics without the first harmonic. The subscript (1) means the first harmonic. The block diagram of the tested CA-CPCT is shown in Fig. 3b.

The aim of SAPF is the elimination of all unwanted components of the load current from the point of view of the presented above current decompositions (1), (2). To achieve SAPF control objectives, the CAs have to generate the following reference current signals:

– according to the PQT (the control algorithm PQT – CA-PQT):

$$\boldsymbol{i}_{ref\mathrm{PQ}} = \boldsymbol{i}_{\overline{q}\mathrm{PQ}} + \boldsymbol{i}_{h\mathrm{PQ}} + \boldsymbol{i}_{2f_{(1)}\mathrm{PQ}} \tag{4}$$

– according to the CPCT (the control algorithm CPCT – CA-CPCT):

$$\boldsymbol{i}_{ref\mathrm{CPC}} = \boldsymbol{i}_{a(\mathrm{h})} + \boldsymbol{i}_s + (\boldsymbol{i}_{r(1)} + \boldsymbol{i}_{r(\mathrm{h})}) + (\boldsymbol{i}_{u(1)} + \boldsymbol{i}_{u(\mathrm{h})}) + \boldsymbol{i}_B \tag{5}$$

4. Experimental results

The complete control system of SAPF consists of: a control algorithm unit, a current controller, a dc voltage controller, a gating signals generator, basic automation functions, etc. has been designed using the rapid prototyping system dSPACE and Matlab/Simulink environment. The developed SAPF control algorithms (CA-PQT, CA-CPCT) have been implemented and tested in the laboratory setup. The topology of the source–load path and SAPF is shown in Fig. 1. The control systems of SAPF

[3] This is decided by the sign of the active power calculated for the given harmonic [11, 12]

have been developed using dSPACE rapid prototyping system, consisting of:

- DS1005 processor board, with signal processor Motorola PowerPC 750, 480MHz,
- DS2002 Multi-Channel A/D board, 32 x 16-bit MUX, 2 ADCs, sim. S&H,
- Digital-I/O Board DS4003, 96 x dig. I/O,
- software: Matlab 5.3, Simulink 3.0, DSP Blockset 3.0 and Control DevelopmentPackage containing Real-Time Interface 3.5.1, ControlDesk 1.2.1, MTRACE/MLIB 4.1.

The main system parameters are:

– supply source:
U_S = 104/60 V, f_S = 50 Hz

– internal impedance of supply source:
$L_S \approx 0.25$ mH, $X_S \approx 79$ mΩ, $R_S \approx 7.9$ mΩ

– 6-pulse thyristor converter:
$R_{Ldc} = 8.82$ Ω, $L_{Ldc} = 18.6$ mH,
dc side and control angle: $\alpha_1 = 50°$, $\alpha_2 = 0°$

– resistive two-terminal network connected between the phases *R* and *S*:
$R_{uRS} = 33.5$ Ω

– shunt active power filter:
$L_{APF} = 1.9$ mH, $C_{APF} = 5$ mF, $UC_{APF,ref} = 320$ V

– switching frequency:
$f_{sw} = 6.4$ kHz

– current PI controller:
$K_p = 0.12$, $K_i = 153.0$

– UC_{APF} voltage PI controller:
$K_{Cp} = 30.0$, $K_{Ci} = 53.2$

In the real power *p* branch (PQT) was applied low-pass (LPF) Butterworth filter 2nd order with cut-off frequency f_c = 25Hz. The selected values result from a compromise between the accuracy of the load current unwanted components elimination and SAPF dynamic behavior. Application of relations formulated in CPCT requires that the complex values of amplitudes of $\underline{\boldsymbol{U}}_{(n)}$ and $\underline{\boldsymbol{I}}_{(n)}$ harmonics[4], being present in the measured voltage and current signals, shall be known. Therefore, in the first place the CPCT based control algorithm performs harmonic analysis of the supply voltage $\boldsymbol{u}_S$ and the load current $\boldsymbol{i}_L$. In order to compute the current components and determine the reference current $\boldsymbol{i}_{ref\text{CPC}}$, a number of operations are performed on the set of the complex values of harmonics amplitudes, determined this way. In the investigation the complex amplitudes of harmonics $\underline{\boldsymbol{U}}_{(n)}$ and $\underline{\boldsymbol{I}}_{(n)}$ were determined using discrete Fourier transform DFT.

The DS2002 board limits the constant switching frequency to 6.4 kHz. This is due to a considerable A/D conversion time of the DS2002 board. With the applied 12-bit resolution, the conversion time for a single channel is minimum 3.8 μs, and for 4 channels supported it gives 15.2 μs (in the experiment 8 channel have been used, 4 per one converter). Also the time required for all computations associated with the control algorithm, as well as with the other elements of the control system, such as: current controller, dc voltage controller, basic automation functions, etc. should be accounted for. The resulting sampling frequency was f_s = 25.6 kHz. For the obtained sampling frequency, a four times lower switching frequency has been defined f_{sw}, ($f_s/f_{sw} = 4$). The control system CS-PQT has been developed using the Simulink standard blocks. The CS-CPCT has been developed using, apart of the Simulink blocks, also the DSP Blockset blocks. The time required to perform all computations for CS-PQT is successively ca. 26 μs, whereas for CS-CPCT this time is ca. 25.4 μs, depending on the 'quality' of the compilation carried out by dSPACE software. The computations for CS-PQT was performed in one time-loop, but for CS-CPCT in two time-loops: a master loop (T_{tt1}), identical for both control systems, restricted by the sampling time T_s = 39.0625 μs, and the slave loop (T_{tt2}), which performs computations related solely to the CA-CPCT. Because of time restrictions, the number *k* of points DFT has been limited to *k* = 32. Thus, in the slave loop, for CA-CPCT, the value of reference current is updated every 625 μs (20 ms/32) – during this time it is held at the constant value (Zero-Order-Hold block). The real time needed for all computations to be carried out in the slave loop is 325 μs, 300 μs still remaining. However, the DSP Blockset toolbox DFT algorithm requires 2^k points. Increasing the number of points to *k* = 64, increases the duration of calculations and at the same time reduces the duration of calculations in the slave time-loop to 312.5 μs (20 ms/64). This was beyond the capacity of the available dSPACE set.

The analysis of APF operation was carried out under conditions of a 'weak' supply system. Fig. 4 shows the waveform and spectrum of the voltage $\boldsymbol{u}_S$, phase *R*, as observed at the terminals of unloaded supply source. The voltage $\boldsymbol{u}_S$ is distorted due to the adverse impact of other non-linear loads connected to the supply system. At the considered PCC this distortion varies within 4-6% $THD\boldsymbol{u}_S$.

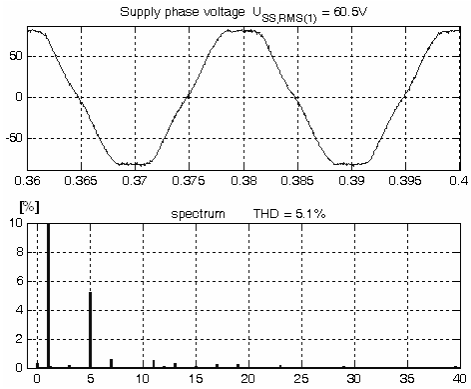

Fig. 4. The waveform of supply voltage u_{SR} and its spectrum, phase *R* – unloaded source supply
Rys. 4. Przebieg napięcia zasilającego u_{SR} i jego spektrum, faza *R* – nieobciążone źródło zasilania

Fig. 5 shows in succession the waveform of the supply voltage u_{SR} and the waveforms of the load current $\boldsymbol{i}_L$ in steady state and dynamic state (step increase, $\alpha_1 = 50° \Rightarrow \alpha_2 = 0°$).

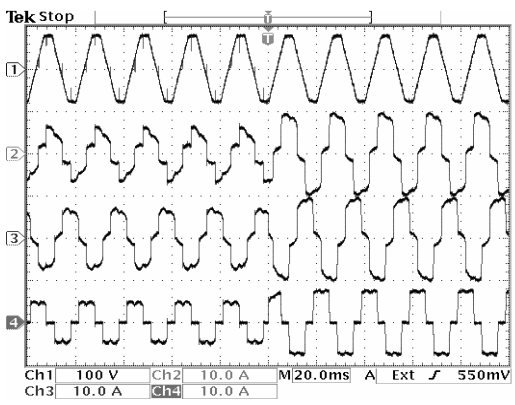

Fig. 5. The waveforms of the supply voltage u_{SR} and the load phase currents i_{LR}, i_{LS}, i_{LT} (current scale × 2)
Rys. 5. Przebiegi napięcia zasilającego u_{SR} i prądów fazowych odbiornika i_{LR}, i_{LS}, i_{LT} (skala prądowa × 2)

[4] $\underline{\boldsymbol{U}}_{(n)} = [\underline{U}_{R(n)}, \underline{U}_{S(n)}, \underline{U}_{T(n)}]^T$, $\underline{\boldsymbol{I}}_{(n)} = [\underline{I}_{R(n)}, \underline{I}_{S(n)}, \underline{I}_{T(n)}]^T$

The load current is unbalanced, distorted and shifted in phase with respect to the voltage $\boldsymbol{u}_S$. The unbalance factor $UF\boldsymbol{i}_L$ is at the level 20.4% for $\alpha_1 = 50°$ and 12.0% for $\alpha_2 = 0°$.

The structure and parameters of the current controllers and the UC_{APF} voltage controllers were identical for both control algorithms. The values of the selected parameters of the investigated source – load path are given in Tab. 1.

Tab. 1. The values of the selected parameters the investigated source - load path before application of SAPF ($UF\boldsymbol{i}$ – unbalance factor)
Tab. 1. Wartości wybranych parametrów badanego układu źródło zasilania – odbiornik przed zastosowaniem SAPF ($UF\boldsymbol{i}$ – współczynnik asymetrii)

		$\alpha_1 = 50°$			$\alpha_2 = 0°$		
phase		*R*	*S*	*T*	*R*	*S*	*T*
$THD\boldsymbol{i}_L$	%	24,84	22,03	30,00	23,74	23,26	28,28
I_L	A	8,50	10,28	7,52	14,18	14,34	11,77
DPF	–	0,887	0,734	0,661	-0,995	0,994	1,000
PF	–	0,856	0,713	0,627	-0,969	0,970	0,963
$UF\boldsymbol{i}_L$	%	20,40			12,00		

The effects of SAPF operation in both the steady and dynamic states are shown in Fig. 6a. Oscilloscope screen images show, consecutively, the waveforms of phase load currents: i_{SR}, i_{SS}, i_{ST}. Enlarged fragments of steady-state waveforms of the current i_{ST} ($\alpha_2 = 0°$) with its spectrum, are presented in Fig. 6b. Subtracting the reference current $\boldsymbol{i}_{ref}$, computed by the given CA, from the load current $\boldsymbol{i}_L$ we obtain the reference signal $\boldsymbol{i}_{Sref}$ for the current at the supply system side (Fig. 6c).

$$\boldsymbol{i}_{Sref} = \boldsymbol{i}_L - \boldsymbol{i}_{ref} \tag{6}$$

CA-PQT

a)

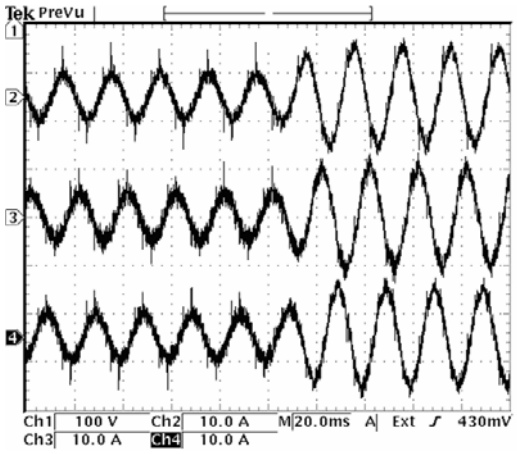

b) c)

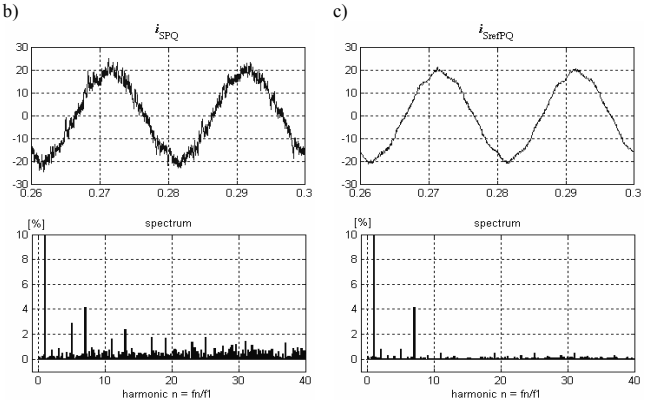

CA-CPCT

a)

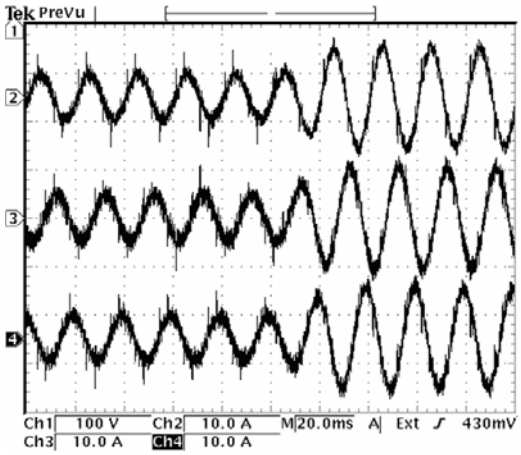

b) c)

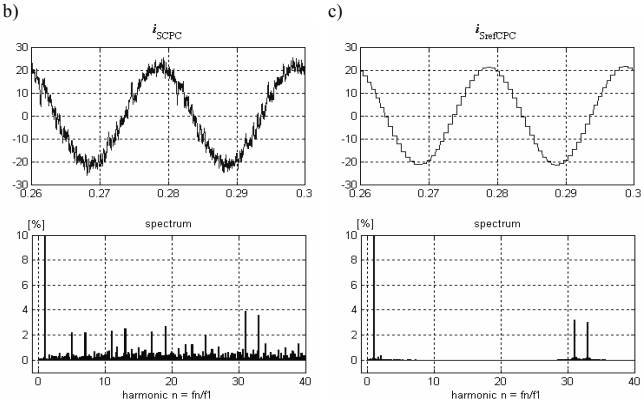

Fig. 6. The waveforms of currents: $\boldsymbol{i}_S$, i_{ST} and i_{SrefT} for CA-PQT and CA-CPCT – experimental results (current scale in Fig. 6a × 2)
Rys. 6. Przebiegi prądów: $\boldsymbol{i}_S$, i_{ST} i i_{SrefT} dla CA-PQT i CA-CPCT – wyniki laboratoryjne (skala prądu na rys. 6a × 2)

The values of selected parameters of the investigated SAPF system at the supply source side are given in Tab. 2.

Tab. 2. The values of the selected parameters after application of SAPF ($UF\boldsymbol{i}$ – unbalance factor)
Tab. 2. Wartości wybranych parametrów po zastosowaniu SAPF ($UF\boldsymbol{i}$ – współczynnik asymetrii)

		$\alpha_1 = 50°$			$\alpha_2 = 0°$		
Phase		*R*	*S*	*T*	*R*	*S*	*T*
CS-PQT – turnaround time: $T_{tt1} = 26\mu s$							
$THD\boldsymbol{i}_S$	%	18,15	16,52	15,65	10,62	9,15	9,33
I_S	A	7,27	7,30	7,26	13,60	13,74	13,61
DPF	–	-0,997	-0,998	-0,998	-0,999	-1,000	-1,000
PF	–	-0,966	-0,957	-0,965	-0,989	-0,988	-0,989
$UF\boldsymbol{i}_S$	%	0,56			0,38		
CS-CPCT – turnaround times: $T_{tt1} = 25.4\mu s$, $T_{tt2} = 325\mu s$							
$THD\boldsymbol{i}_S$	%	17,80	16,13	15,33	10,83	9,25	9,95
I_S	A	7,26	7,26	7,16	14,12	14,19	14,07
DPF	–	0,981	0,978	0,981	0,981	0,979	0,980
PF	–	0,950	0,938	0,948	0,970	0,966	0,969
$UF\boldsymbol{i}_S$	%	0,65			0,48		

CA-PQT

a)

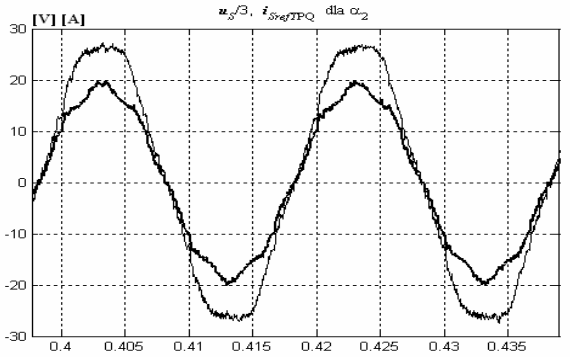

b)

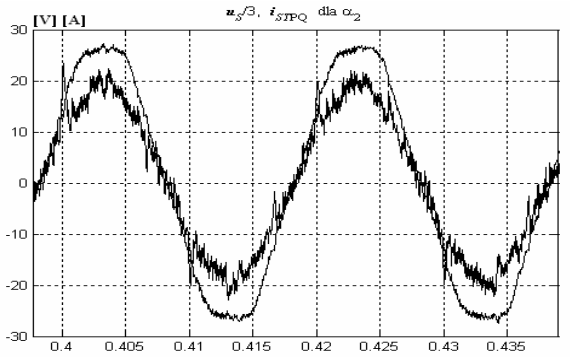

CA-CPCT

a)

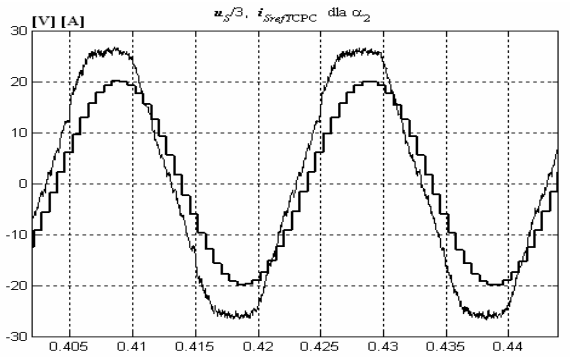

b)

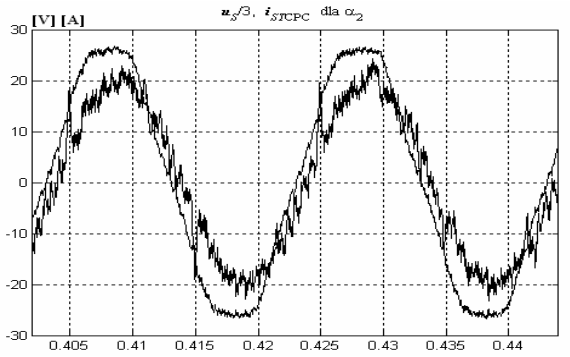

Fig. 7. Enlarged fragments of steady-state waveforms of: the supply voltage u_{ST}, the reference current i_{SrefT} a) and the supply current i_{ST} b) for CA-PQT and CA-CPCT

Rys. 7. Powiększone fragmenty przebiegów w stanie ustalonym: napięcia zasilającego u_{ST}, prądu referencyjnego i_{SrefT} a) i prądu linii zasilającej i_{ST} b) dla CA-PQT i CA-CPCT

From comparing the obtained waveforms of current $\boldsymbol{i}_S$ (Fig. 6) and the values presented in Tab. 2 it can be concluded that:

- the wave shapes of: $\boldsymbol{i}_{SPQ}$ and $\boldsymbol{i}_{SCPC}$ are close to each other and $THD\boldsymbol{i}_S$ values are also close to each other.
- both CAs give the similar results in the supply current balancing.
- SAPF dynamic performance is closely comparable for both CAs. The obtained settling time in response to a step increase of the load current $\boldsymbol{i}_L$ is to 40 ms for both CAs.
- a difference occurs in the results of reactive power compensation. In the event of CA-CPCT, a phase shift occurs between the voltage $\boldsymbol{u}_S$ and current $\boldsymbol{i}_S$ due to the delay caused by the time needed for computing (slave time-loop – 625μs $\Rightarrow$ 11,25° $\Rightarrow$ DPF = 0,981). Enlarged fragments of steady-state waveforms of: the supply voltage u_{SR}, the supply current i_{ST} and the reference current i_{SrefT} for CA-PQT and CA-CPCT are presented in Fig. 7.

The reference current signal $\boldsymbol{i}_{Sref}$ consists of the desired component of the load current $\boldsymbol{i}_L$ and the $\boldsymbol{i}_{APFdc}$ current, needed to replenish the C_{APF} capacitor energy, therefore:

- according to the CS-PQT:

$$\boldsymbol{i}_{SrefPQ} = \boldsymbol{i}_{\bar{p}PQ} + \boldsymbol{i}_{APFdcPQ} \tag{7}$$

- according to the CS-CPCT:

$$\boldsymbol{i}_{SrefCPC} = \boldsymbol{i}_{a(1)CPC} + \boldsymbol{i}_{APFdcCPC} \tag{8}$$

Fig. 6 presents the example waveforms and spectra of currents $\boldsymbol{i}_{Sref}$ from relationships (7)-(8) (right column, $\alpha_2 = 0°$). Differences do occur between the currents $\boldsymbol{i}_S$ at the source side after applying SAPF and the currents $\boldsymbol{i}_{Sref}$ generated by the control systems for the given CA. This is a consequence of a relatively low switching frequency f_{sw} and the lack of passive filtering of the switching frequency component in SAPF current. The currents (7)-(8) differ between themselves, as well. The differences occur in both the wave shapes and in spectra. The $\boldsymbol{i}_{SrefPQ}$ current is distorted because of the $\boldsymbol{u}_S$ voltage distortion. In the $\boldsymbol{i}_{SrefPQ}$ current the 7th harmonic is dominant, though the 5th, 11th, 19th, etc. also occur. The $\boldsymbol{i}_{SrefCPC}$ current waveform approximates the sine-wave with the accuracy determined by the hardware capability. This is related to the above described method of CA-CPCT, where each subsequent value, computed by dSPACE, is updated every 625 μs. Hence, in the $\boldsymbol{i}_{SrefCPC}$ spectrum, beside the first harmonic, also the 31st and 33rd harmonics occur. This is the cause of the $\boldsymbol{i}_{SrefCPC}$ current distortion. Therefore the main cause of the $\boldsymbol{i}_{SrefCPC}$ current distortion is not the supply voltage $\boldsymbol{u}_S$ distortion, but the hardware limitations. It ought to be emphasized that the CA-CPCT worked out the correct reference current $\boldsymbol{i}_{refCPC}$ in spite of the distorted supply voltage at the PCC. It was achieved without using the additional components of CA, such as PLL circuit, signal filter or others. The CA-CPCT was elaborated only on the grounds of the proposed physical interpretation of the phenomena occurring in electrical circuits and the mathematical relationships formulated within CPCT by L. S. Czarnecki.

5. Conclusions

In this paper the comparison of two control algorithms (CAs) of SAPF was presented. The CAs were designed on the basis of: the *p-q* power theory (PQT, CA-PQT) and the power theory based on the current's physical components theory (CPCT, CA-CPCT). The power theory based on the current's physical components took its final form in 1994 [12]. Until now, only its Author has presented

proposals for this theory's practical application [9, 10]. This paper confirms that the power theory based on the current's physical components theory allows developing the control algorithm (CA-CPCT) of SAPF and its practical implementation. The CAs were implemented and tested using the fast prototyping system dSPACE. This hardware and software platform turned out to be a very useful tool for building and developing the control algorithms of SAPF. The laboratory results, with regard to the filtering current harmonics and supply current balancing, are similar for both control algorithms at the given switching frequency of SAPF f_{sw} = 6.4 kHz. Likewise the dynamic performance is comparable in the case of both CAs. The difference occurs in the results of reactive power compensation. In the event of CA-CPCT, a phase shift occurs between the voltage $\boldsymbol{u}_S$ and current $\boldsymbol{i}_S$ due to the delay caused by the time needed for computing (slave time-loop – 625 μs). Significant differences occur between the reference current signals $\boldsymbol{i}_{Sref}$ generated by the CAs. The reasons for the differences between the real $\boldsymbol{i}_S$ and the reference $\boldsymbol{i}_{Sref}$ currents at the source side after applying SAPF are that the laboratory setup has not been equipped with a passive filter for switching frequency elimination and a relatively low switching frequency f_{sw}. The investigation allows the conclusion that the developed algorithm CA-CPCT allows for achieving the supply system current shape close to the sinusoidal, despite SAPF operation under the distorted supply voltage. A sinusoidal supply current cannot be attained by the CA-PQT without some additional control elements, such as: PLL, signal filters, etc. The experiment has shown that testing the capability of SAPF, controlled by the CA-CPCT algorithm, to its full extent requires a controller of a larger computing power. This concerns both the A/D conversion time and harmonic analysis. An alternative solution is the use of a method for harmonic analysis of current and voltage signals different from the discrete Fourier transform DFT. The control algorithm CA-PQT, is certainly easier to implement and less demanding in terms of hardware.

6. References

[1] Akagi H., Kanazawa Y., Nabae A.: "Instantaneous reactive power compensators comprising switching devices without energy storage components", IEEE Trans. on Industry Applications, Vol. IA-20, No. 3, May/June 1984.

[2] Akagi H., Nabae A., Atoh S.: "Control strategy of active power filters using multiple voltage-source PWM converters", IEEE Trans. on Industry Applications, Vol. IA-22, No. 3, May/June 1986.

[3] Akagi H., Nabae A.: "The p-q theory in three-phase circuits under non-sinusoidal conditions", Europ. Trans. on Electric Power, ETEP, Vol. 3, No. 1, pp. 27–31, 1993.

[4] Akagi H., Watanabe E.H., Aredes M.: "The p-q theory for active filter control: some problems and solutions", Sba Controle & Automação, Vol.15, No.1, pp. 78-84, ISSN 0103-1759, Jan./Mar. 2004.

[5] Aredes M., Hafner J. Heumann K.: "Three-phase four-wire shunt active filter control strategies", IEEE Transactions on Power Electronics, Vol. 12, No. 2, pp. 311-318, 1997.

[6] Bhattacharya S., Divan D. M., Banerjee B.: "Synchronous Frame Harmonic Isolator Using Active Series Filter", EPE'91, pp 3-030-3-035, Oct. 1991.

[7] Bhattacharya S., Frank T. M., Divan D. M., Banerjee B.: "Active Filter System Implementation", IEEE Industry Application Magazine, pp. 47-63, September/October 1998.

[8] Chung Se-Kyo: "A Phase Tracking System for Three Phase Utility Interface Inverters", IEEE Transactions on Power Electronics, Vol. 15, No. 3, May 2000.

[9] Czarnecki L. S., Chen G., Staroszczyk Z.: "Application of running quantities for control of adaptive hybrid compensator", European Trans. on Electrical Power, ETEP, Vol. 6, No. 5, pp. 337–344, 1996.

[10] Czarnecki L. S., Hsu S. M., Chen G.: "Adaptive balancing compensator", IEEE Trans. on Power Delivery, Vol. 10 No. 3, pp. 1663–1669, 1995.

[11] Czarnecki L. S.: "Current and power equations at bidirectional flow of harmonic active power in circuits with rotating machines", Europ. Trans. Electr. Power, Vol. 3, No. 1, pp. 45 – 52, ETEP 1993.

[12] Czarnecki L. S.: "Dynamic, power quality oriented approach to theory and compensation of asymmetrical systems under nonsinusoidal conditions", Europ. Trans. Electr. Power, 5, pp. 347 – 358, ETEP 1994.

[13] Emadi A., Nasiri A., Bekiarov S. B.: "Uninterruptible Power Supplies and Active Filters", CRC Press, Illinois Institute of Technology, Chicago, USA, Power Electronics and Applications Series, Series edited by Muhammad H. Rashid, 2005.

[14] Firlit A., Skawiński G.: "Comparison of control algorithms for three-phase three-wire shunt active power filter under distorted supply voltage using dSPACE system", 8th International Conference Electrical Power Quality and Utilisation, Poland, Kraków, EPQU2003, pp. 303-311, 21-23.09.2005.

[15] Firlit A.: „Analiza porównawcza algorytmów sterowania filtrów aktywnych opartych na wybranych teoriach mocy", Rozprawa Doktorska, Akademia Górniczo-Hutnicza, Kraków, 2006.

[16] Firlit A.: „The active power filter operation under the distorted supply voltage", 11th International Conference EPE2005, Drezno, CD-No. 0686, 02-04.09.2005.

[17] Monteiro L.F.C., Aredes M.: "A Comparative Analysis among Different Control Strategies for Shunt Active Filters," in Proc. (CDROM) of the V INDUSCON – Conferęncia de Aplicações Industriais, Salvador BA, Brazil, pp. 345-350, 03-05 July 2002.

[18] Moran L., Dixon J., Wallace R.: „A three-phase active power filter operating with fixed switching frequency for reactive power and current harmonic compensation" IEEE Tran. on Power Industrial Electronics, Vol. 42, No 4, August 1995.

[19] Pasko M., Maciążek M., Dębowski K.: „Kompensacja wpływu odbiorników nieliniowych na sieć zasilającą niskiego napięcia", Przegląd Elektrotechniczny, R.80, str. 807-812, 9/2004.

[20] Pasko M., Maciążek M.: „Aktywna kompensacja równoległa w układach trójfazowych czteroprzewodowych", Przegląd Elektrotechniczny, R.80, str. 544-548, 6/2004.

[21] Pasko M., Maciążek M.: „Teoria mocy p-q poprawna teoria czy użyteczny algorytm sterowania kompensatorów kluczujących", Przegląd Elektrotechniczny, R.82, 6/2006.

[22] Pasko M., Maciążek M.: „Wkład elektrotechniki teoretycznej w poprawę jakości energii elektrycznej", IC-SPETO'2004, tom I, ss. 5a-5k, (referat monograficzny) lub Wiadomości Elektrotechniczne. Nr 7-8, str. 37-46, 2004.

[23] Pasko M., Walczak J.: „Optymalizacja energetyczno-jakościowych właściwości obwodów elektrycznych z przebiegami okresowymi niesinusoidalnymi", Z. N. Pol. Śl. „Elektryka", z. 150, monografia, Gliwice, 1996.

[24] Pasko M.: „Opis właściwości energetycznych, energetyczno-jakościowych obwodów elektrycznych z przebiegami niesinusoidalnymi okresowymi", Przegląd Elektrotechniczny, Nr 59, str.23-40, 2002.

[25] Rashid M. Dixon J., Moran L.: „Power Electronics Handbook, Chapter 33 Active Filters", Academic Press, August 2001.

Artykuł recenzowany